A new method to trace colloid transport pathways in macroporous soils using X-ray computed tomography and fluorescence macrophotography

Diego Soto-Gómez[1,2], Paula Pérez-Rodríguez[1,2,3], Laura Vázquez Juíz[1,2], J. Eugenio López-Periago[1,2], and Marcos Paradelo[4]

[1]Soil Science and Agricultural Chemistry Group, Department of Plant Biology and Soil Science, Faculty of Sciences, University of Vigo, E-32004 Ourense, Spain.

[2] Hydraulics Laboratory, Campus da Auga, Facultade de Ciencias, Campus da Auga, University of Vigo.

[3]Laboratory of Hydrology and Geochemistry of Strasbourg (LHyGeS)
Université de Strasbourg, Strasbourg, France.

[4]Department of Sustainable Agriculture Sciences, Rothamsted Research, Harpenden, Herts, United Kingdom

Correspondence. D. Soto-Gómez. Email: disoto@uvigo.es

Running title: A method to trace colloid transport pathways in soils

This article has been accepted for publication and undergone full peer review but has not been through the copyediting, typesetting, pagination and proofreading process, which may lead to differences between this version and the Version of Record. Please cite this article as doi: 10.1111/ejss.12783

Summary

The fast and deep percolation of particles through soil is attributed to preferential flow pathways, and their extent can be critical in the filtering of particulate pollutants in soil. Particle deposition on the pore walls and transport between the pores and matrix modulate the preferential flow of particulate pollutants. In the present research, we developed a novel method of combining fluorescence macrophotography and X-ray computed tomography (CT) to track preferential pathways of colloidal fluorescent microspheres (MS) in breakthrough experiments. We located accumulations of MS by fluorescence imaging and used them to delimit the deposition structures along the preferential colloid pathways by superimposing these images on the 3-D pore network obtained from CT. Advection–diffusion with transport parameters from the dual-porosity equation correlated with preferential pathway features across different soil management techniques. However, management did not influence the morphology of the MS preferential pathways. Preferential flow occurred in only a small fraction of the total pore network and was controlled by pores connected to the soil surface and by matrix density.

Keywords: particulate tracer; pore descriptors; tillage; pore connectivity; preferential pathways.

Highlights:

- X-ray tomography and epifluorescence images were combined to identify preferential pathways in soil.
- Preferential pathways constituted approximately 1 % of the soil bulk volume.
- Correlations between descriptors of preferential pathways and colloid transport were found.
- Tillage influenced the morphology of pores, but not the shape of preferential pathways.

1. Introduction

Macropores are generally recognized to facilitate rapid long-range transport of particulate matter through the soil profile (Beven & Germann, 2013), causing agronomic, environmental, health and engineering issues. For example, deep percolation of particulate contaminants and nutrients results in groundwater contamination and reduces crop yields (de Jonge et al. 2004). Application of manures and urban wastes to soil can lead to contamination of groundwater with pathogenic microorganisms, which occurred in Ontario in 2000 when thousands of people became seriously ill (Hrudey et al. 2003). In recent years, there has been an increase in the domestic use of engineered nanoparticles (Babakhani et al. 2017), which has coincided with their release into sewage (Benn et al. 2010) and the environment (Hoppe et al. 2015). The presence of these harmful colloids in treated wastewater for irrigation (Russo et al. 2014) is a risk to human health and the environment (Molnar et al. 2015). In environmental engineering, the performance of novel remediation techniques for soil contaminated with organic materials, metals or halogenated organic compounds using nano- and micro-particles (Mueller & Nowack 2010) depends on accessibility to the contaminated soil sites (Pan & Xing, 2012).

The theory of colloidal transport in granular collectors is well developed (see Elimelech et al. (1995) and references therein). However, transport in structured soils is still being studied. Linking the soil structure to transport is a large challenge that started three decades ago and continues because of the complex relations among spatial heterogeneity, variable chemical properties and scale (Bejat et al. 2000). Advances in this field need to collect detailed information on the soil structure and porosity together with transport information from breakthrough experiments with dyes, unreactive tracers and microspheres. For example, the results of the experiments performed by Burkhardt et al. (2007) and Flury & Wai (2003) are controversial: Burkhardt et al. found that transport properties depend on the pore-space geometry, whereas Flury and Wai gave more importance to the water content or the pore-water velocity. Köhne et al. (2009) reviewed the state of the art for modelling preferential flow and physical nonequilibrium transport under transient conditions. The above authors concluded that structure-related information, namely, macroporosity,

connectivity, tortuosity and surface area of the matrix, among other descriptors, is relevant to describe colloid transport. Moreover, the spatial arrangement of the soil pores has a strong influence on the transport of solutes and colloids (Vogel et al., 2010), as well as the fraction of macropores that transmit particles (Passmore et al. 2010; Burkhardt et al. 2007). Nielsen et al. (2011) showed that biopores promoted deep transport. Koch et al. (2016) found that titanium (IV) oxide (TiO_2) colloids, with an average size of 0.3 μm, were transported exclusively by macropores using both root and earthworm channels. In the same research, a soluble dye tracer travelled through the matrix but reached greater depth via macropores, where the dye percolated to a depth similar to that of TiO_2. These findings support the notion that pore network connectivity and biopores should be considered to describe particle transport in structured soil.

In addition to the above, soil structure is not static; agricultural practices can dramatically modify the soil pores with further influence on transport (Bronick & Lal, 2005). Tillage breaks the aggregates and disrupts the continuity of large biopores and replaces them with cracks and repacked pores or with massive structures without macropores. In addition, soil compaction by machinery traffic and tillage instantly modify the organization of pores (Horn 2004). However, porosity reorganizes after a few years with no-tillage or minimum tillage practices (Zurmühl & Durner, 1996).

Several techniques, such as water or air percolation and tracer leaching (Shipitalo et al. 2000), are used to study the effects of tillage on physical soil properties. However, in recent decades CT techniques have been successfully applied to examine the effect of soil management on the pore architecture (Ambert-Sanchez et al. 2016) and to study tracer transport in different types of soil (Paradelo et al. 2016). Descriptors of morphological, statistical and fractal properties can be studied together with other physical properties to describe soil functions (Naveed et al., 2013; San José Martínez et al., 2014).

Following this approach, in a previous article (Soto-Gómez et al. 2018) we reported significant correlations among macroscopic descriptors of CT porosity, soil physical properties and some

parameters of the advection–diffusion equation with dual porosity. These correlations suggested the importance of particle trapping on the macropore walls. Therefore, we hypothesized that information on an individual macropore basis obtained from the location of preferential pathways and deposition sites in transport experiments can provide details about colloid transport in structured soil-pore networks.

In the present research, we aimed to be more precise and to study only the pores that can transmit microspheres. Therefore, our main objective was to develop a method for the identification of preferential pathways for microsphere transport in soils with different pore networks, using macrophotography of fluorescent particles and CT. These techniques have not been combined in any previous research as far as we know. We also studied the pores connecting the top of the soil to the bottom (potential preferential pathways) and examined the effect of agricultural management on the characteristics of the particle transport pathways extracted with the method proposed.

2. Materials and methods

2.1. Soil sampling and breakthrough experiments

The general procedures for soil sampling, CT scanning and breakthrough experiments were described in Soto-Gómez et al. (2018); therefore, they are only briefly explained here. In the present study, sixteen undisturbed soil columns (100-mm height × 84-mm diameter) were sampled from two adjacent experimental plots (Centro de Desenvolvemento Agrogandeiro, Ourense, NW Spain, coordinates 42.099N –7.726W WGS84): eight columns from a plot devoted to organic agriculture with more and less earthworm activity deduced in the field from the signs of surface alteration (named Org. A and Org. B, respectively), four columns from a plot of spring cereal with no-till after sowing and with the roots of the crop preserved (Conv. NT) and four columns from a shallow-tilled plot (Conv. ST). We had two types of sampling: probability sampling performed randomly over the plots to obtain the Conv. NT, Conv. ST and Org. B samples, and non-probability sampling in the

case of Org. A. In this last case, the samples were chosen deliberately in parts of the plot where we observed more earthworm activity, to test the most favourable scenario for particle transport. Our experimental design involved pseudoreplication rather than true replication. Nevertheless, we consider that statistical analysis is justified because our three plots were large and adjacent so that they shared most of their characteristics.

The samples were taken vertically, discarding the vegetation cover (2–12-cm depth). The chemical properties of the soils from the different plots were very similar, with coefficients of variation in general less than 5 %, with a pH of 5.9 (with a standard error of 0.05) in a 1:10 soil:water mixture. Moreover, all soils had the same sandy loam texture.

After sampling, the columns were stored at 4ºC before analysis. Samples were scanned by X-ray CT with a dental scanner, 3-D Cone-beam i-CAT (Imaging Sciences International LLC, Hatfield, PA) using 120 kV, 5 mA current and a voxel size of 0.24 mm. The software Image-J version 1.52a (Rasband 2012) was used to analyse the raw data and extract properties such as the CT porosity (i.e. the percentage of pores larger than 0.24 mm extracted from the computed tomography images), the connectivity (calculated through the Euler characteristic) (Toriwaki & Yonekura, 2002) and the surface and volume of the pores (Soto-Gómez et al. 2018). We considered that pores below the CT resolution (240 μm) are the micro- and meso-pores that constitute the porosity of the matrix. The CT pores that connected from top to bottom through the soil column were separated using the 3-D object counter (Bolte & Cordelières 2006). The bounding box features (smallest box encompassing the object) allowed identification and characterization of the connecting pores.

For the breakthrough experiments, red fluorescent polystyrene latex microspheres (MS) of 1 ± 0.11 μm (Magsphere Inc., Pasadena, CA) were used as colloidal tracers. We used a suspension of 2.28×10^8 microspheres ml^{-1} in a solution of 0.025 M Br^- (KBr). The water content of columns during breakthrough was close to saturation with an effective saturation of 0.92 ±0.03, and the flow boundary conditions were a constant flux at the upper boundary with a flow rate of ~10 ml $hour^{-1}$ (5.1 mm $hour^{-1}$) and a seepage face at the bottom. The flow rate was reduced in some columns (nos

9, 10, 15 and 19) to avoid surface ponding resulting from the decrease in infiltration at late stages of the breakthrough (for further information, see Soto-Gómez et al. (2018)). Water and microsphere suspensions were distributed thoroughly dropwise at random points across the topsoil surface by a robotic arm attached to a dripper connected to a peristaltic pump (Minipuls III pump, Gilson Inc., Middleton, WI).

Before the breakthrough experiments, drip irrigation with deionized water (DW) was applied to the columns until the flow rate at the seepage face and turbidity of the outflow were undetectable. After reaching stable conditions, a pulse of the MS suspension was applied (≈ 2–3 pore volumes, PV), followed by 10 PV of MS-free DW. The volume of effluent collected (≈ 4–6 ml per tube) was determined by weighing, [Br^-] was measured by automated colorimetry (van Staden et al. 2003) and the particle concentration was determined by fluorescence spectroscopy (Jasco Fluorescence Spectrometer, Jasco FP-750, Japan). The porosity and bulk density used in the flow calculations were determined from the soil columns after drying and after microsphere counting and pathway identification.

2.2. Microsphere counting and pathway identification

Once the breakthrough experiments had been performed, the columns were sliced into 5-mm sections with a nylon string and a spatula. A piston jack and a precision Vernier caliper were used to extrude the soil from the PVC casing in 5-mm steps. Fluorescence macrophotographs from the upper end of each soil slice were taken in a dark room (Figure 1a). The light excitation source was a green laser module 10 mW and 532 nm (Edmund Optics. Inc. Stock No #84-929, Barrington, NJ) coupled to a cone beam expander (Edmund Optics Inc. Stock No #58-272) and a 24° diffusion angle speckle reducer (Edmund Optics Inc. Stock No #88-393). Fluorescence images were taken with a digital camera (Canon EOS 400D, Tokyo, Japan) with an exposure of 5 s and a sensitivity of ISO-200. The camera objective (55 mm) was coupled to a dichroic filter passband between 592 and 635 nm with a 43 nm bandwidth (Edmund Optics Inc. serial No #67-048) (Figure 1a). Thus, the

stained zones where the microspheres accumulated were identified. No microsphere counting was performed in the images because of the self-quenching effect; the tendency of the fluorescent dyes to reabsorb the emitted fluorescence when the concentration of fluorophores is large (Klauth et al. 2007). The images were taken at 16 Mpixel resolution, which allowed the detection of microsphere aggregates larger than 30 µm. The fluorescence images were segmented using the Otsu threshold (Otsu 1979) in Image-J to obtain the proportion of stained surface in each image. The Otsu method assumes that the images have two types of pixels (black and white) and it separates them by considering the minimum intraclass variance and the maximum interclass variance.

Once the images had been taken, the slices were transported in Petri dishes to identify microsphere accumulations under a fluorescence laboratory magnifier. In each slice, the soil pore walls stained by microspheres (see Figure 1a) were collected with perforating punches and stored in centrifuge vials. The rest of the soil slice was stored separately in a bottle. The contents of the tubes and bottles were weighed. Then, the microspheres retained both in the contour of the macropores and in the soil matrix were quantified separately as follows: 10 ml (pore walls) or 20 ml (matrix) of a nonionic surfactant solution (Tween 20 in distilled water, 0.02 %) was added to their respective vials or bottles to increase the dispersion and stability of the suspensions and to avoid aggregation of the MS. The suspensions were shaken and homogenized for 10 s by ultrasonication. Aliquots (0.5 ml each, three replicates) were immediately pipetted and diluted in appropriate volumes of 0.02 % Tween 20 and filtered through nitrocellulose membranes (pore size 0.45 µm, diameter 47 mm). The particles were counted in the filter using digital images obtained with a fluorescence laboratory magnifier and a digital camera (Figure 1b). With this method, we calculated the percentages of MS retained in the matrix (% MS matrix) and in the pore walls (% MS pores) of the total MS. Image processing was performed with Image-J, using supervised thresholding to identify the microspheres and the Bone-J Particle Analyzer plugin for counting the individual microspheres.

A fraction of microspheres that passed through soil pores was attached to the pore walls. This feature was used to track the MS pathways along the CT pore network. The 3-D reconstruction of

the pathways from fluorescence images cannot provide the precise geometry required for further analyses. Moreover, with CT images only it is not possible to identify the actual preferential flow paths. Therefore, fluorescence stains and CT images were combined to increase the quality of the reconstructed microsphere pathways; this is a novel procedure that involves the merging the stacks of binary images of macropores (from CT) and MS fluorescence stains (from macrophotographs). First, the two stacks were scaled and aligned using the reference marking notches in the column casing. We used the Simple Neurite Tracer plugin, implemented in ImageJ (Longair et al. 2011), to trace the microsphere pathways. The tracing started by locating the centre of a fluorescent spot in the bottom image of the MS stack. Then, the same point in the CT stack (at the same depth) was selected, and the path started only if the point belonged to a macropore. The next step was to move to the slice of the MS fluorescence stack immediately above and repeat the operation. If the new microsphere spot was located in the same pore identified previously in the CT stack, the software drew the trajectory of the MS pathway by choosing the voxels with a similar shade (dark = pore) across the images in the CT stack. The process continued to the upper end of the sample until a skeleton of the MS pathways was obtained.

The Bone-J software collected information on junctions, branches and lengths (Euclidean distances and real length) of the macropore skeletons, which were stored as vectors. The vector information on the microsphere paths across the CT stack described the ‘skeleton’ of the colloidal transport pathways, which is the thin version of the path shape. Sequences of 3-D dilations over the skeleton (Figure 2a) were performed and then overlapped with the binary CT images to define the shape of the conducting MS pores (% MS paths) (Figure 2b). With this technique, we calculated the proportion of connected CT pores used by the particles to travel across the column (% MS connected paths), the disconnected pores used (% MS disconnected paths) and the proportion (MS disconnected/MS connected). Figure 2(c and d) shows examples of the 3-D representation of the skeleton and the filled pores of the MS pathways, respectively.

2.3. Statistical analysis

The normality of the variables was tested using the Kolmogorov–Smirnov test. Four variable had non-normal distributions: % MS paths, % MS connected paths, % MS disconnected paths and the proportion MS disconnected/MS paths. Differences in soil characteristics regarding management were evaluated by one-factor analysis of variance ANOVA (Sthle & Wold 1989). We checked that all residuals were normally distributed with the Kolmogorov–Smirnov test. The correlations between the variables studied were calculated by Pearson's method. The % MS paths values were transformed to the natural logarithm of the value + 1, and the proportion MS disconnected/MS paths values were transformed to square roots. To simplify the interpretation of the article the transformed values of the properties were not included in the tables, but the correlations were calculated with the transformed values where necessary. All analyses were performed using the software R (R Development Core Team 2011).

3. Results and discussion

3.1. Connected CT porosity

Features of the pore networks and skeletons extracted from the CT images are summarized and explained in Table 1. We considered some of these features, but we focus on the connection of CT pores and pathway properties. The values obtained for each property describing these features are shown in Table 2.

Figure 3 shows representative examples of the pore network, one for each tillage treatment. We found that the total CT porosity and the CT porosity considering only the pores connecting the top of the soil column to the bottom were strongly correlated (Pearson's r = 0.99). This strong correlation shows that the structure of the macropore network is arranged in such a way that it contributes mostly to the vertical connectivity along the entire column. The CT porosities showed significant differences between the tillage treatments. The number of connected pores in the Conv.

ST plot (Figure 3b) were not significantly different from the other plots, but there was more intragroup variability, 6.7 % (3.4 %), and a denser zone (without CT pores) in the lower part of the core, which corresponded to the maximum depth of the shallow tillage. The Org. A plot (Figure 3c), with more earthworm activity, had a significantly larger percentage of connecting pores, 8.4 % (2.2 %), than the other two plots: NT, 4.1 % (1.4 %) and Org. B, 3.3 % (1.9 %). The Conv. NT plot (Figure 3a) had many root pores and some isolated earthworm pores, whereas the Org. B plot had the fewest connecting paths.

Computed tomography connectivity did not show significant differences between zones but was slightly greater in the conventional plots and values were smallest in the Org. B columns. This feature was directly related to the retention of bromide (r = 0.61) and indicated that the number of connections increased the storage of bromide. In general, the number of connections indicates the existence of more paths, more branches and, in the majority of cases, more dead-end properties that can enhance the exchange of solutes between the macropores and the matrix.

3.2. Fluorescence macrophotographs

The analysis of the fluorescence macrophotographs showed no correlation between the stained area and the retention of microspheres in the column after the breakthrough experiments (r = 0.08). In the Org. B samples, most of the retention occurred in the pore walls (concentration was six times larger than that in the matrix); at the same time, the stained area in the matrix decreased. The average percentages of the stained areas were significantly different ($P < 0.05$) between treatments: Org. B columns had the smallest stained area (9.5 ± 0.5 %), followed by NT (12.7 ± 0.7 %), ST (14 ± 1.1 %) and Org. A (14.9 ± 2.4 %) zones.

Figure 4(a) shows a strong correlation (r = 0.71) between the stained area and the CT porosity. It results from the penetration of microspheres in the matrix through the pore walls. Moreover, microspheres penetrate a few tenths of millimeters into the matrix surrounding the pores. This

penetration has already been reported for dyes (Cey & Rudolph, 2009). The correlation slightly improved when only the proportion of CT pores connecting from the top to the bottom of the soil were considered (Figure 4b). Table 3 gives a summary of the correlation coefficients. Excluding the root pores from the above analysis, decreased the correlation between CT porosity and the stained area to Pearson's $r = 0.42$. This difference supports the interpretation that root channels contribute to the transport of microspheres and is consistent with other research that showed that roots increased dye transport with water content close to saturation (Liu et al. 2016).

3.3. Microsphere pathways

Examples of the 3-D reconstruction of MS pathways that connect the tops with the bottoms of the soil columns are displayed in Figures 5(a–d). It is noteworthy that the MS were encountered in both connected and disconnected pores. In the second case, the MS enter into the disconnected pores through the micro- and meso-pores of the soil matrix. The volume of stained pores represents only a small fraction of soil volume (1.25 ± 0.9 %) and one-fifth of the CT-porosity volume.

For all the pathway characteristics studied (see Tables 1 and 2 for descriptions and summary), only the maximum branch length showed significant differences regarding soil management. Soils from NT plots had longer paths (77.8 ± 19.1-mm length) because of the high density of root channels. In the Org. A soil, paths had an intermediate length (58.6 ± 12 mm) mostly consisting of earthworm burrows. However, the maximum branch lengths of MS paths were shorter in Org. B (36.2 ± 22.5 mm) and ST (46.3 ± 7.7 mm) soils because of less earthworm activity in the former and the greater disruption of paths by tillage in the latter. The other pathway descriptors and the mass balance of transport of MS did not differ between the types of soil tillage, which suggests that preferential flow occurred in macropores with similar morphology. Moreover, some of the pores that connected from top to bottom appeared to start or end in the wall of the column (between the soil and the carcass), a problem that arises from sampling in soil with a large biopore density. This effect could account for

the similar mass balance between the types of soil tillage. However, the shape of MS preferential pathways and the surface stained were reasonably independent of that effect.

The correlation between the percentage volume of stained CT-pores (% MS Paths) and the percentage of stained area in the soil slices (Figure 6a) suggests that fluorescence macrophotography provided good estimates of the CT pores acting as preferential MS pathways. Figure 6(b, c) shows strong inverse relations between retention (MS and Br^-) and the ratio MS disconnected/MS connected described in Table 1. Figure 6(b) suggests that increasing the ratio of connecting pores decreased colloid retention in soil, and indicates that deposition of MS in the matrix occurred mainly in the columns with the smallest CT porosity (Org. B and Conv. ST). Conversely, in the Org. A and Conv. soils, which had the smallest matrix density, the microspheres were transported through the matrix, but in this case, deposition of MS on the disconnected macropores was less. We hypothesized that in these soils the matrix flow transporting MS did not pass through the disconnected macropores. Evidence for the transport of particles through the matrix has been reported in similar experiments in artificial soils with poorly connected macroporosity (Lehmann et al. 2018) and with repacked soils (Darnault et al., 2017). The authors of this last study noted that *Cryptosporidium parvum* oocysts (with diameters 3 to 5 times larger than the microspheres used here) moved through the matrix of sandy loam soil in small numbers. Because the soil used in our study had textural and chemical properties similar to those of the above reference, the movement of smaller particles through the matrix is feasible.

4. Conclusions

We have presented a novel method to trace the preferential transport pathways of microspheres in soils with different types of macropores that were identified by computed tomography. The soil management techniques produced CT pores with different morphologies. However, the differences were not significant when we analysed the morphologies of preferential microsphere pathways using the same descriptors, i.e. these preferential pathways were independent of soil management.

Earthworm pores, cracks and root pores led to different spatial distributions of particle deposition sites, but their occurrence did not influence the mass balance of microspheres. Soil bulk density and pore continuity affected the spatial distribution of microspheres trapped in the soil matrix.

The first results obtained with the method presented, based on the combination of X-ray computed tomography and fluorescence macrophotography, outline the importance of transport across macropore walls. They reinforce current knowledge about links between soil structure and colloid transport. Further development of this method will contribute to a better understanding of the transport of colloids in structured soils, and will help in several fields such as the assessment of bacterial transport and colloidal pollution, remediation with reactive engineered particles and development of soil management strategies to control deep percolation of particulate nutrients and contaminants.

5. Acknowledgments

The authors acknowledge the following funding sources: D.S.G. is funded by the Predoctoral Fellowship Program (FPU) of Spain's Ministry of Education FPU14/00681, P.P.R is funded by a postdoctoral fellowship awarded by Xunta de Galicia (Gain program ED481B-2017/31), L.V.J. is funded by CITACA ED431/07 and BV1 research contracts (FEDER, *Xunta de Galicia*) and M.P is supported by the BBSRC-funded Soil to Nutrition strategic program (BBS/E/C/000I0310). The authors thank the Centro de Desenvolvemento Agrogandeiro (Ourense) for allowing the sampling in their plots and Oscar Lantes at the archeometry unit RIADT-CACTUS services USC for the CT image acquisition with their dental 3-D Cone-beam i-CAT scanner. This research was partially funded the INOU 2018 (Universidade de Vigo).

6. References

Ambert-Sanchez, M., Mickelson, S. K., Ahmed, S. I., Gray, J. N. & Webber, D. 2016. Evaluating soil tillage practices using X-Ray computed tomography and conventional laboratory methods. *Transactions of the ASABE*, *59*, 455–463.

Babakhani, P., J. Bridge, R. A. Doong & Phenrat, T. 2017. Parameterization and prediction of nanoparticle transport in porous media: A reanalysis using artificial neural network. *Water Resources Research*, *53*, 4564–4585.

Bejat, L., Perfect, E., Quisenberry, V. L., Coyne, M. S. & Haszler, G. R. 2000. Solute transport as related to soil structure in unsaturated intact soil blocks. *Adsorption Journal of The International Adsorption Society, 64,* 818–826.

Benn, T., Cavanagh, B., Hristovski, K., Posner, J. D. & Westerhoff, P. 2010. The release of nanosilver from consumer products used in the home. *Journal of Environmental Quality*, *39*, 1875–1882.

Beven, K. & Germann, P. 2013. Macropores and water flow in soils revisited. *Water Resources Research*, *49*, 3071–3092.

Bolte, S. & Cordelières, F. P. 2006. A guided tour into subcellular colocalization analysis in light microscopy. *Journal of Microscopy*, *224,* 213–232.

Bronick, C.J. & Lal, R. 2005. Soil structure and management: A review. *Geoderma*, *124,* 3–22.

Burkhardt, M., Kasteel, R. , Vanderborght, J. & Vereecken, H. 2007. Field study on colloid transport using fluorescent microspheres. *European Journal of Soil Science*, *59,* 82–93.

Cey, E. E. & Rudolph, D. L. 2009. Field study of macropore flow processes using tension infiltration of a dye tracer in partially saturated soils. *Hydrological Processes*, *23,* 1768–1779.

Darnault C. J. G., Peng, Z., Yu, C., Li, B., Jacobson, A. R. & Baveye, P. C. 2017. Movement of cryptosporidium parvum oocysts through soils without preferential pathways: Exploratory test.

Frontiers in Environmental Science, 5. doi:10.3389/fenvs.2017.00039

de Jonge, L. W., Kjaergaard, C. & Moldrup, P. 2004. Colloids and colloid-facilitated transport of contaminants in soils. *Vadose Zone Journal*, *3*, 321–325.

Elimelech, M., Gregory, J., Jia, X. & Williams, R.A. 1995. *Particle Deposition & Aggregation*. , Butterworth–Heinemann (Elsevier), Woburn, MA.

Flury, M. & Wai, N. N. 2003. Dyes as tracers for vadose zone hydrology. *Reviews of Geophysics*, *41,* 1002.

Hoppe, M., Mikutta, R., Utermann, J., Duijnisveld, W., Kaufhold, S., Stange, C. F. & Guggenberger, G. 2015. Remobilization of sterically stabilized silver nanoparticles from farmland soils determined by column leaching. *European Journal of Soil Science*, *66,* 898–909.

Horn, R. 2004. Time dependence of soil mechanical properties and pore functions for arable soils. *Soil Science Society of America Journal*, *68,* 1131–1137.

Hrudey, S. E., Payment, P., Huck, P. M., Gillham, R. W. & Hrudey E. J. 2003. A fatal waterborne disease epidemic in Walkerton, Ontario: Comparison with other waterborne outbreaks in the developed world. *Water Science and Technology*, *47,* 7–14.

Klauth, P., Bauer, R., Ralfs, C., Ustohal, P., Vanderborght, J., Vereecken, H. et al. 2007. Fluorescence macrophotography as a tool to visualise and quantify spatial distribution of deposited colloid tracers in porous media. *Colloids and Surfaces A: Physicochemical and Engineering Aspects*, *306*, 118–125.

Koch, S., Kahle, P. & Lennartz, B. 2016. Visualization of colloid transport pathways in mineral soils using titanium(IV) oxide as a tracer. *Journal of Environmental Quality*, *45,* 2053–2059.

Köhne, J. M., Köhne, S. & Šimůnek, J. 2009. A review of model applications for structured soils: a) Water flow and tracer transport. *Journal of Contaminant Hydrology*, *104*, 4–35.

Lehmann, K., Schaefer, S., Babin, D., Köhne, J. M., Schlüter, S., Smalla, K. et al. 2018. Selective transport and retention of organic matter and bacteria shapes initial pedogenesis in artificial soil—A two-layer column study. *Geoderma*, *325,* 37–48.

Liu, H., Janssen, M. & Lennartz, B. 2016. Changes in flow and transport patterns in fen peat following soil degradation. *European Journal of Soil Science*, *67*, 763–772.

Longair, M. H., Baker, D. A. & Armstrong, J. D. 2011. Simple neurite tracer: Open source software for reconstruction, visualization and analysis of neuronal processes. *Bioinformatics*, *27*, 2453–2454.

Molnar, I. L., Johnson, W. P., Gerhard, J. I., Willson, C. S. & O'Carroll, D. M. 2015. Predicting colloid transport through saturated porous media: A critical review. *Water Resources Research*, *51,* 6804–6845.

Mueller, N. C. & Nowack, B., 2010. Nanoparticles for remediation: Solving big problems with little particles. *Elements*, *6,* 395–400.

Naveed, M., Moldrup, P., Arthur, E., Wildenschild, D., Eden, M., Lamandé, M. et al. 2013. Revealing soil structure and functional macroporosity along a clay gradient using X-ray computed tomography. *Soil Science Society of American Journal*, *77,* 403–411.

Nielsen, M. H., Styczen, M., Ernstsen, V., Petersen, C. T. & Hansen, S. 2011. Distribution of bromide and microspheres along macropores in and between drain trenches. *Vadose Zone Journal*, *10*, 345–353.

Otsu, N. 1979. A threshold selection method from gray-level histograms. *IEEE Transactions on Systems, Man, and Cybernetics*, *9,* 62–66.

Pan, B. & Xing, B. 2012. Applications and implications of manufactured nanoparticles in soils: A review. *European Journal of Soil Science*, *63,* 437–456.

Paradelo, M., Katuwal, S., Moldrup, P., Norgaard, T., Herath, L. & de Jonge, L. W. 2016. X-ray CT-

derived soil characteristics explain varying air, water, and solute transport properties across a loamy field. *Vadose Zone Journal*, *15*. https://doi.org/10.2136/vzj2015.07.0104

Passmore, J. M., Rudolph, D. L., Mesquita, M. M. F., Cey, E. E. & Emelko, M. B. 2010. The utility of microspheres as surrogates for the transport of *E. coli* RS2g in partially saturated agricultural soil. *Water Research*, *44,* 1235–1245.

R Development Core Team, R. 2011. *R: A Language and Environment for Statistical Computing*. R Foundation for Statistical Computing, Vienna.

Rasband, W. 2012. *ImageJ. U. S. National Institutes of Health, Bethesda, Maryland, USA*, p.//imagej.nih.gov/ij/.[Accessed November 13, 2018].

Russo, T., Alfredo, K. & Fisher, J. 2014. Sustainable water management in urban, agricultural, and natural systems. *Water*, *6*, 3934–3956.

Shipitalo, M. J., Dick, W. A. & Edwards, W. M. 2000. Conservation tillage and macropore factors that affect water movement and the fate of chemicals. *Soil & Tillage Research, 53*, 167–183.

Soto-Gómez, D., Pérez-Rodríguez, P., Vázquez-Juiz, L., López-Periago, J. E. & Paradelo, M. 2018. Linking pore network characteristics extracted from CT images to the transport of solute and colloid tracers in soils under different tillage managements. *Soil& Tillage Research, 177*, 145–154.

van Staden, J. F., Mulaudzi, L. V. & Stefan, R. I. 2003. On-line speciation of bromine and bromide using sequential injection analysis with spectrophotometric detection. *Analytical and Bioanalytical Chemistry, 375,* 1074–1082.

Ståhle, L. & Wold, S. 1989. Analysis of variance (ANOVA). *Chemometrics and Intelligent Laboratory Systems, 6,* 259–272.

Toriwaki, J. & Yonekura, T. 2002. Euler number and connectivity indexes of a three dimensional digital picture. *Forma*, *17,* 183–209.

Vogel, H.-J., Weller, U. & Ippisch, O. 2010. Non-equilibrium in soil hydraulic modelling. *Journal of Hydrology, 393*, 20–28.

Zurmühl, T. & Durner, W. 1996. Modeling transient water and solute transport in a biporous soil. *Water Resources Research, 32*, 819–829.

Table 1. Summary and description of the variables studied.

Property	Description
CT porosity/%	†Percentage of the volume occupied by the *CT pores.
Connected CT porosity/%	†Percentage of CT pores connecting the top surface of the soil column to its bottom.
Connectivity	The number of connected structures in the pore network, determined by calculating the Euler characteristic of the CT pore skeleton.
Bulk density/g cm $^{-3}$	Mass of air-dried soil per unit of bulk volume.
MS and Br Retained/%	‡Percentage mass of microspheres and bromide retained in the soil column at the end of a breakthrough experiment.
MS matrix/%	‡Percentage of microsphere mass retained in the soil matrix with respect to the total concentration.
MS pores/%	‡Percentage of microsphere mass retained in the CT pore walls with respect to the total concentration.
Average stained surface/%	Percentage of soil slice covered by fluorescent stains calculated as the average percentage of all slices per soil column.
MS paths/%	†Percentage of pore volume with walls coated with microspheres (see methods 2.2 section).
MS connected paths/%	†Stained pores connecting the top surface of the soil column to its bottom.
MS disconnected paths/%	†Stained pores not connecting the soil column from top to bottom.
MS disconnected/ MS paths	Ratio of not connecting stained CT pores referred to the total stained pores expressed as a volume ratio.
MS paths skeleton properties	Properties of the skeleton of the microsphere pathways, including the number of branches, junctions, tortuosity and total, average and maximum branch length.

*CT pores are those pores bigger than 0.24 mm extracted from the computed tomography images.
†Volume of CT pores is related to the bulk soil volume expressed in percentage.
‡Percentage is related to the mass of MS or Br^- injected into the column during the breakthrough experiments.

Table 2: Average of the properties studied and the parameters obtained from the analysis of variance.

Soil Management	CT porosity/%	Connected CT porosity/%	Bulk density /g cm $^{-3}$	MS Retained/%	Br Retained/%	MS pores/%	MS matrix/%
Conv. ST	7.56	6.70	1.44	37.53	12.42	5.15	32.38
Conv. NT	4.65	4.06	1.49	40.99	14.58	5.59	36.30
Org. A	9.52	8.38	1.44	47.41	13.50	11.48	35.93
Org. B	4.34	3.31	1.47	31.47	7.45	7.71	23.76
SE	1.26	1.17	0.02	9.50	3.06	2.20	8.41
F	3.83	4.06	1.44	0.49	1.06	1.73	0.48
P	0.04	0.03	0.28	0.69	0.40	0.21	0.70
LSD	3.90	3.59	–	–	–	–	–

Soil Management	Average Stained Surface/%	MS Paths/%	MS Disconnected Paths/%	MS Connected Paths/%	MS Disconnected / MS Paths	MS Paths: Maximum Branch Length /mm
Conv. ST	14.00	1.97	0.07	1.90	0.04	46.30
Conv. NT	12.76	0.92	0.02	0.90	0.05	77.78
Org. A	14.93	1.53	0.02	1.51	0.01	58.64
Org. B	9.52	0.58	0.08	0.50	0.15	36.19
SE	0.70	0.40	0.03	0.40	0.03	8.19
F	11.32	2.32	0.93	2.45	2.25	4.77
P	0	0.12	0.47	0.11	0.16	0.02
LSD	2.16	–	–	–	–	25.25

Conv. ST, conventional agriculture shallow tilled; Conv. NT, conventional agriculture with no-till after sowing; Org. A, organic agriculture with more earthworm alteration; Org. B, organic agriculture with less earthworm alteration; CT, computed tomography; MS, microspheres; SE, standard error; and LSD, least significant difference (calculated for a Student's $t_{p=0.05}$).

Table 3. Summary of the correlation coefficients.

	CT Porosity/%	Connected CT pores/%	MS Retained/%	Br Retained/%	Average Stained Surface/%	MS Paths/%	MS Disconnected/ MS Paths
CT porosity/%	1.000						
Connected CT pores/%	**0.995**	1.000					
MS Retained/%	n.s.	n.s.	1.000				
Br Retained/%	n.s.	n.s.	*0.772*	1.000			
Average Stained Surface/%	*0.711*	**0.748**	n.s.	n.s.	1.000		
MS Paths/%	**0.745**	**0.772**	n.s.	n.s.	0.599	1.000	
MS Disconnected/ MS Paths	n.s.	–0.511	–0.525	*–0.660*	*–0.635*	n.s.	1.000

Bold face indicates correlations are significant at 0.1% level.

Italic face indicates correlations are significant at 1% level.

n.s. not significant > 0.5% level

The MS paths/% values were transformed to the natural logarithm, and the proportion MS disconnected/MS paths values were transformed to square roots.

CT, computed tomography; MS, microspheres.

7. Figures

Figure 1. (a) Schematic diagram of the employed system to make fluorescence photographs of the cross-sections of the soil column. The photographs were used to identify the deposition sites of fluorescent microspheres (MS) after the breakthrough experiments. Excitation light was a green laser module 532 nm coupled to a beam expander and a 24º diffusion angle speckle reducer. The camera objective was attached to an optical passband filter between 592–635 nm, 43 nm bandwidth. Accumulations of microspheres appear as orange fluorescence stains around the pore walls in the raw image. Background green colour is shown intentionally as a reference only in this photograph; this was obtained with a less selective long-pass optical filter (> 590 nm) that allowed some of the reflected laser light by soil to reach the camera sensor and (b) example of fluorescence microphotography used for quantification of MS retained in the filter (red dots).

(a)

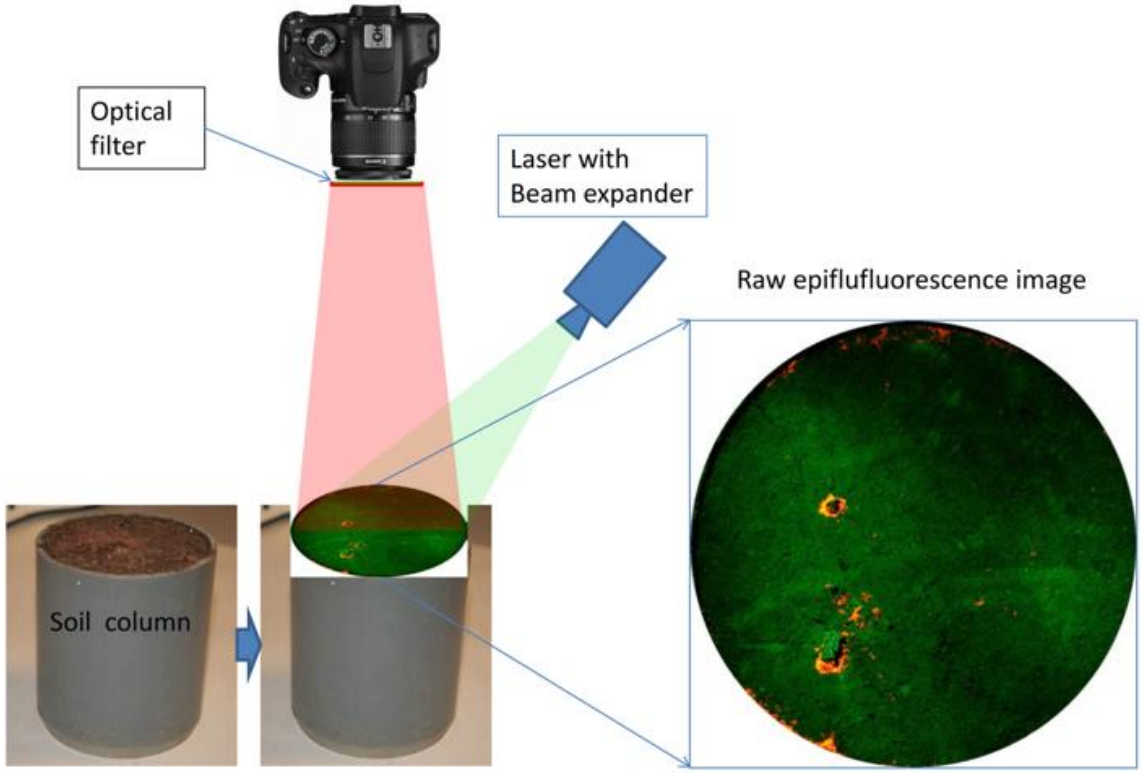

(b)

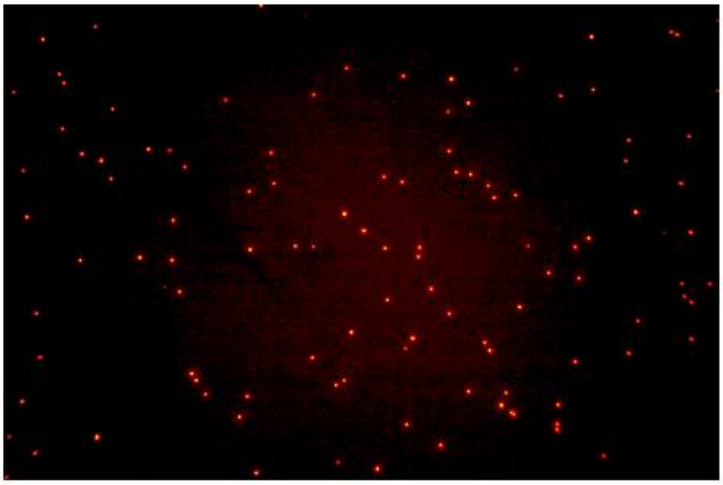

Figure 2. Sample images of the MS pathway identification procedure: (a) detail of a slice of the pathway skeleton dilated (black), (b) cross-section of combined CT pores and the fluorescent paths showing the pores not used by the MS (in black), the CT pore paths used by the MS connecting from top to bottom (in light blue) and paths used by MS, but not connecting the top to the bottom (in dark blue), (c) 3-D view of the MS pathway skeleton and (d) 3-D representation of the entire volume of the MS pathways.

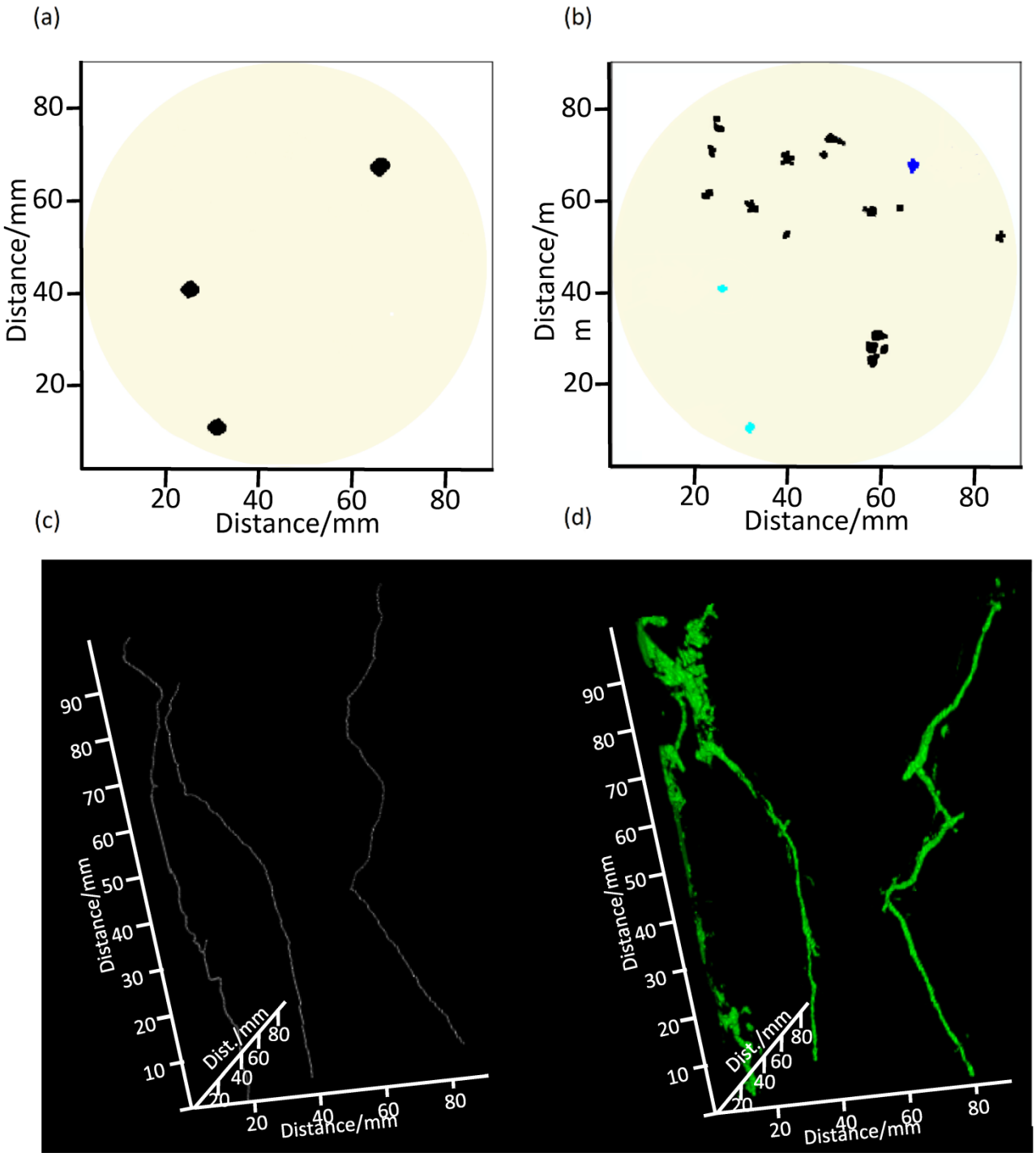

Figure 3. 3-D representation of the CT pores of four columns representing each of the four macropore structures: (a) conventional with no-till after sowing (Conv. NT), (b) conventional shallow till (Conv. ST), (c) organic agriculture–more earthworm alteration (Org. A) and (d) organic agriculture–less earthworm alteration (Org. B). The full-connecting pores from top to bottom are shown in blue and the disconnected ones in pink. The box frame in white indicates the scale in the three dimensions; perspectives were optimized for viewing so that axis lengths in the image differ from their actual sizes.

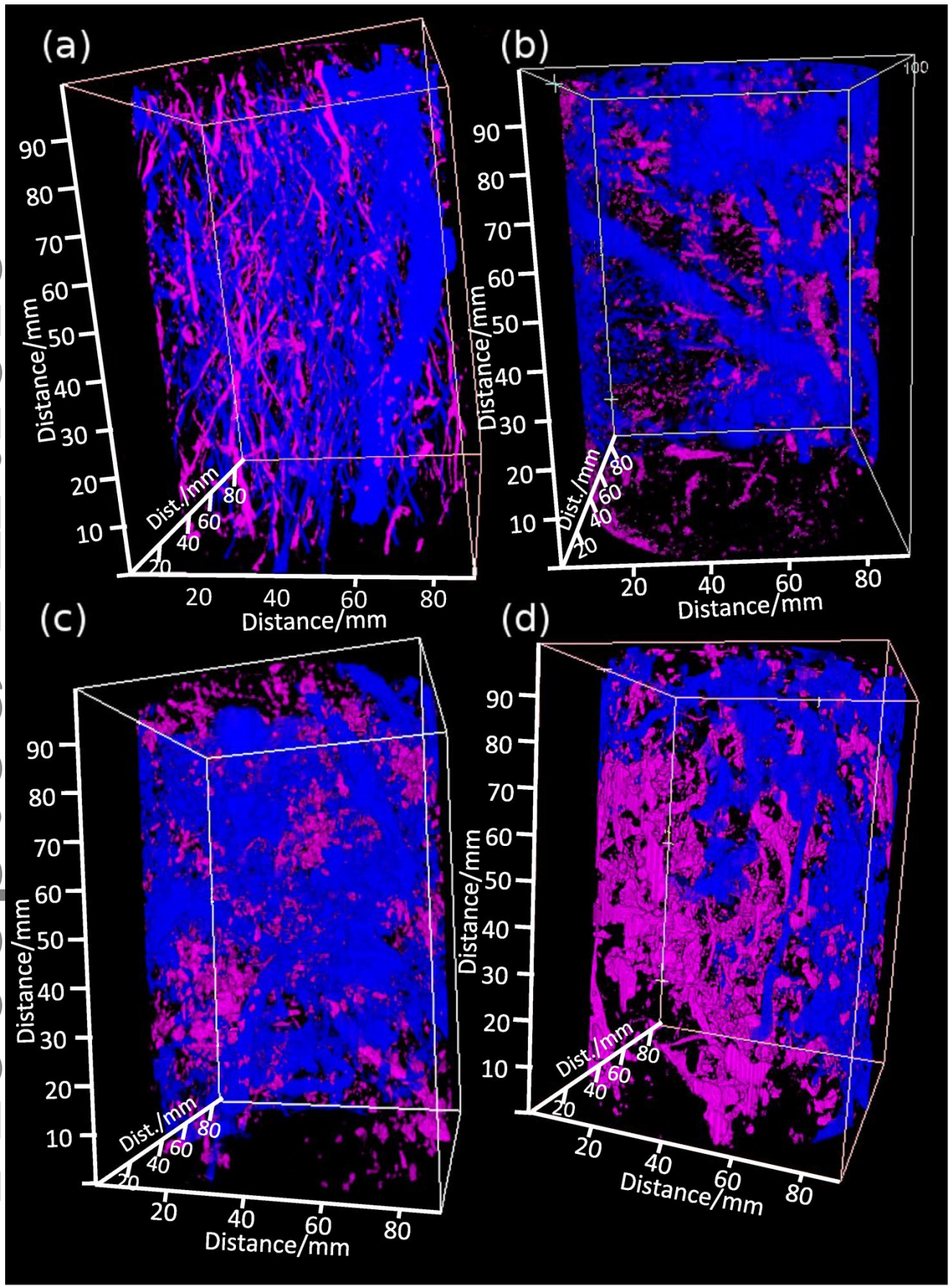

Figure 4. Correlation between the average of the percentage area stained by microspheres in the fluorescence macrophotographs (a) the total CT-porosity and (Pearson's $r = 0.71$) and (b) the CT porosity connected from top to bottom ($r = 0.75$) (both percentages are referred to the pore volume regarding the bulk soil volume).

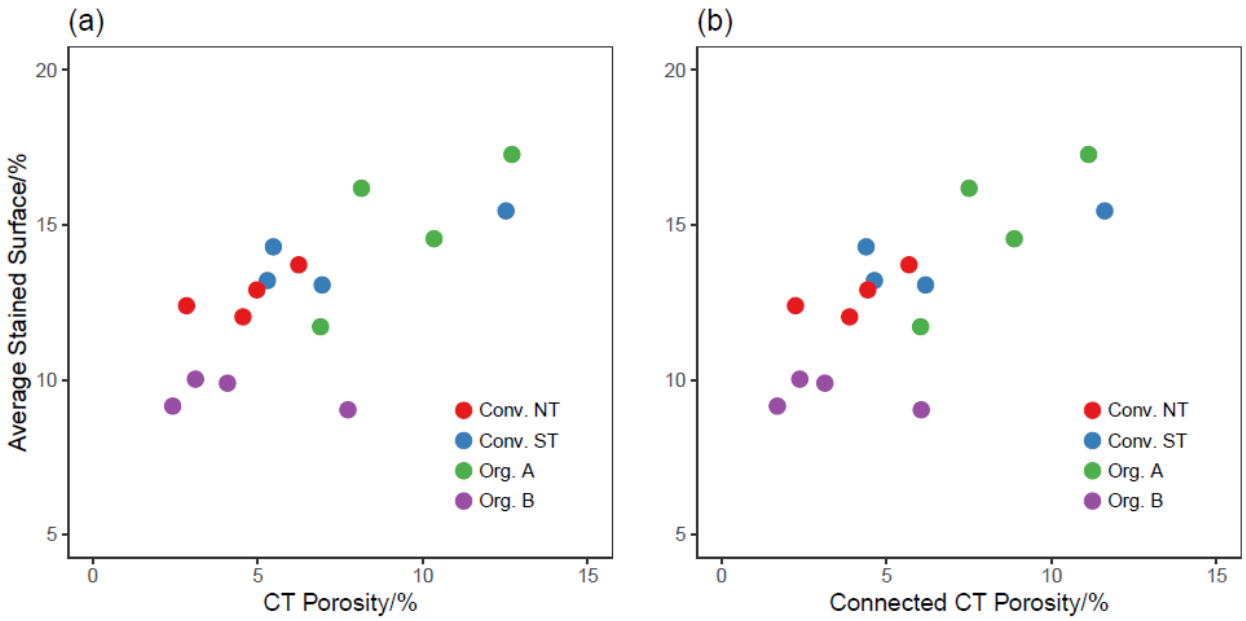

Figure 5. 3-D representations of the colloid pathways in four soil columns: (a) Conv. NT, (b) Conv ST, (c) Org. A and (d) Org. B. The connecting pores from top to bottom are in white (Connected CT pores). The MS-connecting paths from top to bottom are light blue and the MS paths that do not connect are in dark blue. Conv. NT, conventional with no-till after sowing; Conv. ST. conventional shallow till; Org. A, organic agriculture with more earthworm alteration; Org. B, organic agriculture with less earthworm alteration

(a)

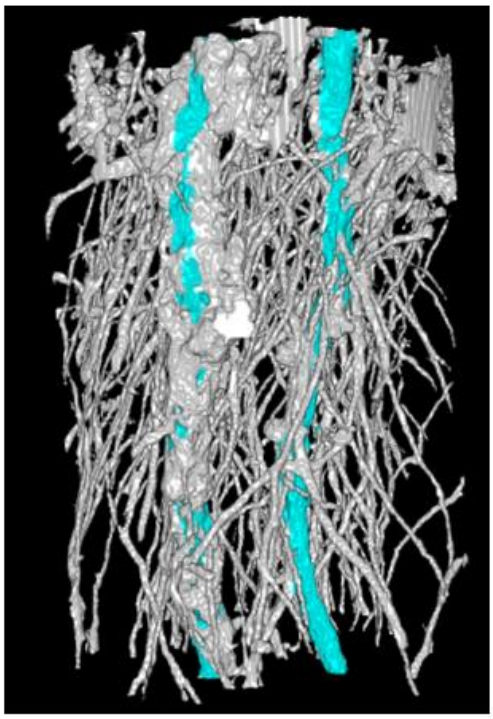

(b)

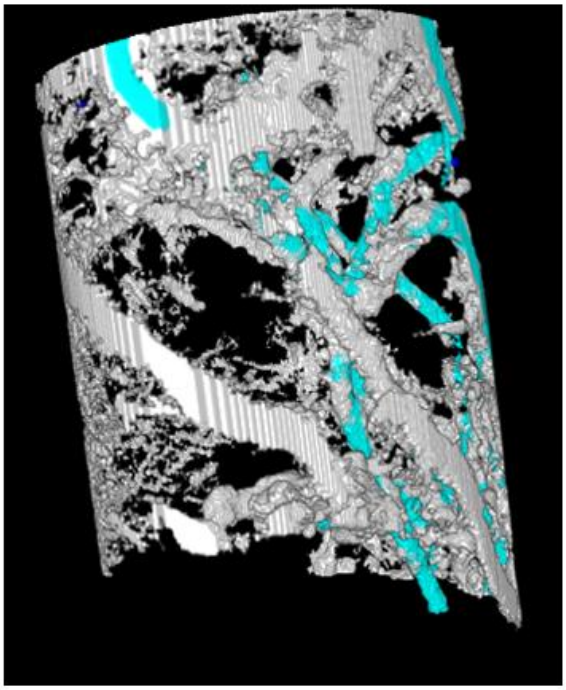

(c)

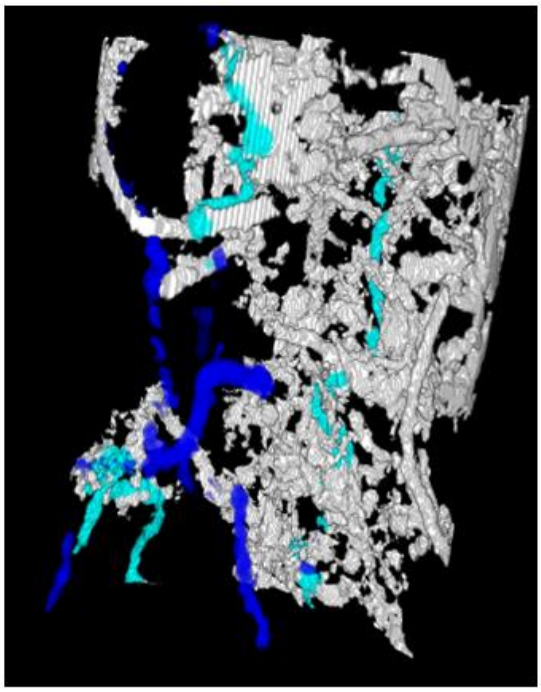

(d)

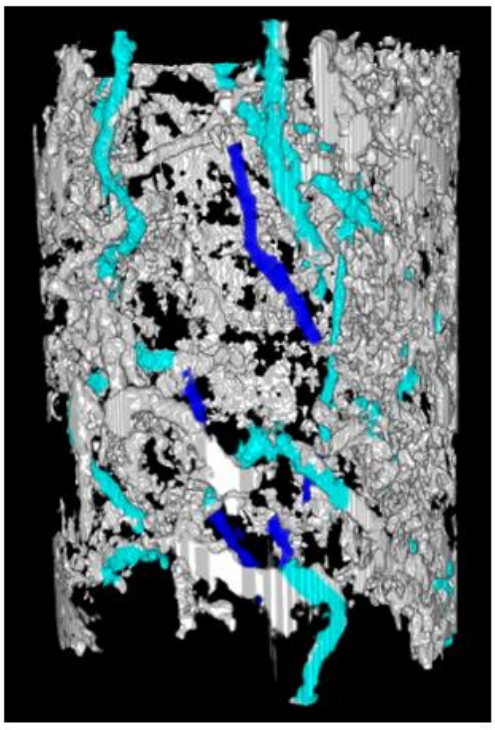

Figure 6. Relations between (a) percentage of pore volume forming MS paths and percentage of the average stained surface in fluorescence photographs (r = 0.60), (b) percentage of MS particles retained in the column and percentage of disconnected CT pores forming MS paths (r = 0.54) and (c) percentage of bromide retention and proportion of disconnected MS paths (in relation to the total MS paths) (r = 0.66).